JOURNAL OF APPLIED ELECTROCHEMISTRY 20 (1990) 186–195

Potential distribution and electrode stability in a bipolar electrolysis cell

J. DIVISEK, R. JUNG

Institute of Applied Physical Chemistry, Nuclear Research Centre, Jülich, 5170 Jülich, FRG

D. BRITZ

Kemisk Institut, Aarhus Universitet, 8000 Aarhus C, Denmark

Received 23 January 1989; revised 12 June 1989

A computational model is presented, which enables the identification of those zones endangered by corrosion in a bipolar electrolysis cell stack. The method consists of two steps: first the potential profile in the electrolyser is computed by numerical solution of the Laplace equation using the finite difference method; then, making use of the Criss–Cobble correspondence principle, this profile is related to the potential-dependent thermodynamic stabilities of the respective metals. This may be a useful tool in the design of intermittently operating electrolysers (for example those powered by solar energy).

Nomenclature

A	metal phase
A_i	single A-phase point
B	electrolyte phase
B_i	single B-phase point
F	Faraday constant
h	mesh interval (m)
i	local current density ($A\,m^{-2}$)
i_0	exchange current density ($A\,m^{-2}$)
j	local current across the double layer (A)
j_{iA}, j_{iB}	tangential or normal component of the double layer current (A)
K	A, B phase conductivity ratio
m	molality $mol\,kg^{-1}$
R	gas constant
T	absolute temperature (K)
U	potential (V)
U_0	water decomposition voltage (V)
U_{tot}	end plate potential (V)
x, y	cartesian coordinates
α	overrelaxation factor
η_a, η_c	anodic or cathodic overpotential (V)
κ_A, κ_B	electrical conductivity ($\Omega^{-1}\,m^{-1}$)
Φ	potential (V)
Φ_m	local double layer potential, electrode end (V)
Φ_s	local double layer potential, electrolyte end (V)

1. Introduction

A bipolar electrolyser is an electrical system with a complex equivalent circuit; parallel with the desired current, at least two other parasitic currents flow through it. The corresponding potential and current distribution can depend strongly on the operating conditions in the cell (fully or partially loaded, or switched off). Potential distributions may occur in the system such that the catalysts or cell construction materials employed suffer mild or even destructive corrosion. Corrosion is a rather more serious effect of potential distribution than the mere existence of the parasitic currents themselves. The main cause of these undesirable phenomena are the electrolyte inlet and gas outlet channels which, however, must be included in a cell design. In order to obtain a better understanding of the conditions in such a bipolar cell, an analysis was carried out, combining thermodynamic stability data for the relevant materials with the potential profile within the electrolyser. With the aid of a two-dimensional diagram, such an analysis enables the identification of those cell areas endangered by corrosion.

2. Description of the method

The technique will be demonstrated using the advanced water electrolyser as an example. Such cells may be used in the future in combination with solar cells, producing hydrogen, and will run intermittently, because of the diurnal cycle. For this reason, this class of electrolyser, frequently switched off, will be especially prone to corrosive effects.

The newer, cathodically effective, catalysts are based on the structure of Raney nickel. To increase efficiency and stability, d-metals with at most five electrons in the d-orbital can be added to this catalyst, according to the Jaksić interpretation of the Brewer–Engel valence bond theory [1]. The best known of such metals is molybdenum, with its one 5s and five 4d electrons. The most common electrolyser construction material is steel, with Fe as main component. Fig. 1 shows the thermodynamically calculated solubility of

0021-891X/90 $03.00 + .12

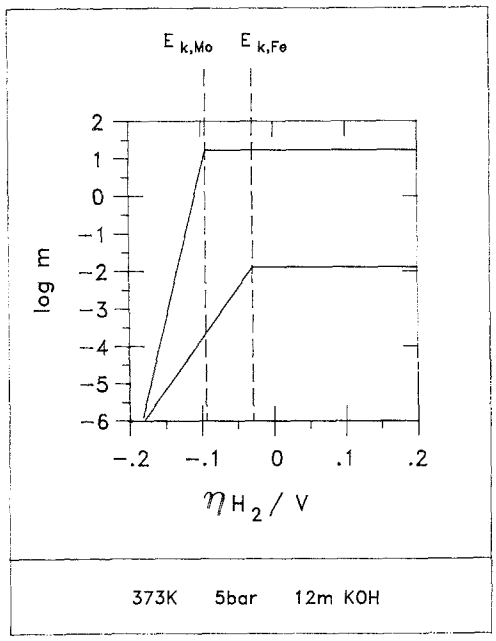

Fig. 1. Thermodynamic stability of Fe and Mo in 12 m KOH (as their solubility m) as a function of the hydrogen overpotential η_{H_2}; critical potential E_k. The solubility is determined by the solubility product.

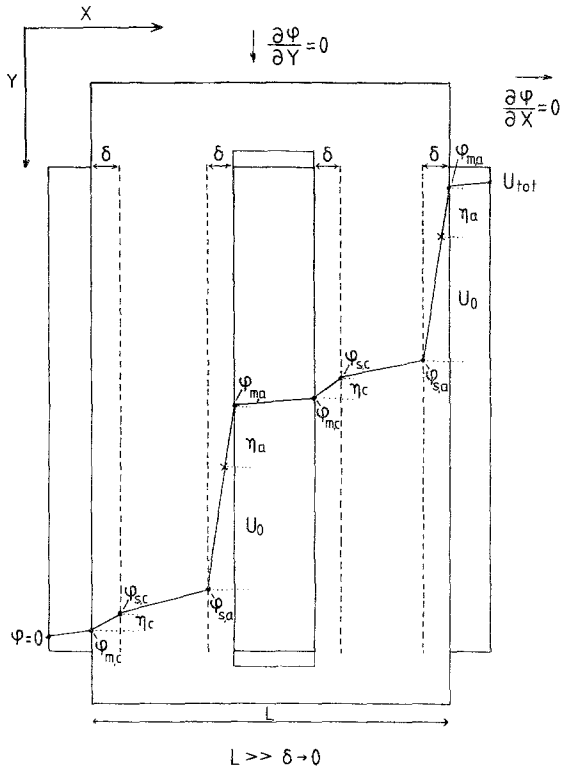

Fig. 2 Two-dimensional schematic of the bipolar electrolyser. The electrochemical double layer thickness is δ, assumed to approach zero.

both these metals as $\log m$ against the hydrogen overpotential, η_{H_2}, for typical operating conditions of advanced water electrolysis. Details of this calculation will be given in a latter publication; here, it will serve to show a model functional connection between the maximum solubility of the two metals Fe and Mo and the corresponding local hydrogen overpotential η_{H_2}, as a computer-calculated cross-section of the relevant Pourbix-type diagram [2]. Figure 1 shows only the region of active dissolution of pure Fe and Mo. An analogous diagram for the anodic region is unnecessary, since here one uses passivated pure Ni, whose oxohydrate surface has negligible solubility [3]. If the thermodynamic stability for a given metal, seen in Fig. 1, is coupled with known cell potential profiles, those regions endangered by corrosion can then be topologically identified.

3. Calculation of potential profile

Figure 2 shows a two-dimensional schematic of a bipolar electrolyser with, for the time being, just a single plate. The cathodic end is assigned the potential zero, while the anodic end plate has potential U_{tot}. The electric double layer comprises point Φ_s (electrolyte) and Φ_m (metal). For the cathodic double layer we have $\Phi_{s,c}$ (electrolyte) and $\Phi_{m,c}$ (metal) and, analogously, for the anodic double layer, we have $\Phi_{s,a}$ and $\Phi_{m,a}$, respectively. Local potential differences $\Delta\Phi_c = \Phi_{s,c} - \Phi_{m,c}$ and $\Delta\Phi_a = \Phi_{m,a} - \Phi_{s,a}$ are unknowns at present. However, for zero current

$$\Phi_{s,c} - \Phi_{s,a} = U_0 \tag{1}$$

must hold between opposite sides of a bipolar plate. U_0 here is the pressure- and temperature-dependent decomposition voltage of water. This additive constant U_0 can be arbitrarily distributed between $\Delta\Phi_c$ and $\Delta\Phi_a$, but it is of practical value to assign it fully to the anodic side. In this case we have, for the cathodic and anodic overpotential at zero local current ($i = 0$), the definition

$$\Delta\Phi_c = 0; \quad \Delta\Phi_a = U_0 \tag{2}$$

and, for finite current density $|i| > 0$

$$-\eta_c = \Delta\Phi_c; \quad \eta_a = \Delta\Phi_a - U_0 \tag{3}$$

The electrolyser schematically shown in Fig. 2 can be described in cartesian coordinates. The potential field in the homogeneous phases is then in the form of the Laplace equation in two dimensions

$$\frac{\partial^2\Phi}{\partial x^2} + \frac{\partial^2\Phi}{\partial y^2} = 0 \tag{4}$$

The numerical solution of this equation for given boundary conditions is well understood [4, 5]. Generally, four methods are popular:

1. The resistor network method; the 2-D space is modelled as a network of resistors ([6], cited in [7]), and Kirchhoff's rule is applied to each mode. The resulting matrix equation is solved. Solutions are obtained in a matter of seconds, but point spacing needs to be rather rough.

2. The finite difference method (FDM): the field space is modelled by a set of sampled points, usually spaced equidistant and the Laplace Equation 4 is discretized at each point. The solution is the steady state to which one converges after a number of iterations, at each of which each point is updated. so as to conform to the discrete form of the Laplace equation.

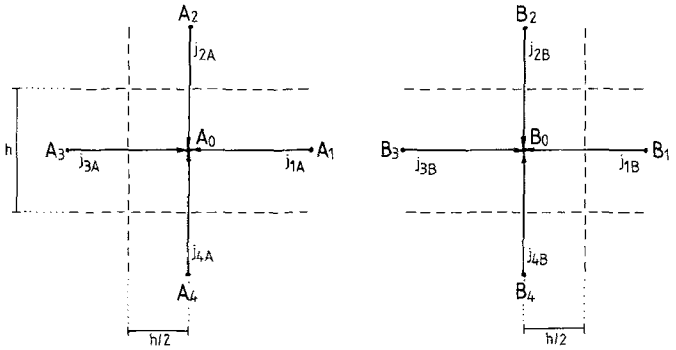

Fig. 3. Schematic representation of boundary between two Laplacian regions.

3. The finite element method (FEM): one takes advantage of the fact that there are large areas in the potential field where large point spacing is acceptable. One places a number of sample points in the field such that they are close together where the field is strongly curved and more widely spaced elsewhere. The total number of points is then considerably smaller than with the FDM, and the problem – after considerable mathematical effort – reduces to the solution of a matrix equation of reasonable size. This has been used by many workers, among them Holmes and White [7] and Dimpault-Darcy and White [8].

4. The boundary integral element method (BIEM): this promises even smaller matrix equations, only points on the field boundaries need to be treated. Good references here are [4] and [9], the latter focussing on electrochemical applications.

Method 1, the resistor network model, produces approximate results. The FDM was chosen by us, despite its characteristically long computation times (but see below). The cell space is placed in an equispaced point mesh and both Equation 4 and boundary conditions are written as discrete approximations and solved iteratively. The discretization schemes can be explained with reference to Figs 3 and 4. Applying

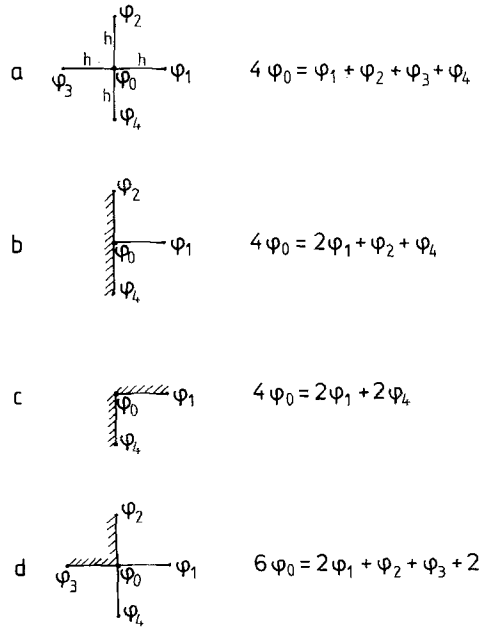

Fig. 4. Discrete finite difference forms of the Laplace equation in two dimensions, at various places in the cell: (a) homogeneous field; (b) a smooth edge; (c) an inner corner; (d) an outer corner.

Kirchhoff's rule to total elemental current – that is, multiplying current densities by elemental (in some cases fractional) areas – we have, for the homogeneous bulk phase, Fig. 4a, the approximation for Equation 4

$$4\Phi_0 = \Phi_1 + \Phi_2 + \Phi_3 + \Phi_4 \qquad (5)$$

for a mesh with equal intervals h in both x and y (see [4]).

These equations correspond to the simple mesh star arrangement in Fig. 3 (either A or B) (see [4]). For the electrolyte/electrode and electrolyte/insulator interphases, the following conditions hold: for phase A, the left-hand star A is appropriate and for phase B, the right-hand star B. The interphase runs through the points A2, A0 and A4 of star A and through the points B2, B0 and B4 of star B. The point A3 lies wholly in phase A; point A1 is hypothetical. Symmetrically opposite these, phase B has corresponding points B1 and hypothetical B3. The potentials $\Phi_i(A)$ at point A_i and $\Phi_i(B)$ at point B_i are referred to the cathodic end-plate potential ($\Phi = 0$). Then we have, for the local currents j_{iA} and j_{iB}, the relations

$$\left.\begin{aligned} j_{iA} &= \frac{\kappa_A}{h}[\Phi_0(A) - \Phi_i(A)]\frac{h}{2} \\ j_{iB} &= \frac{\kappa_B}{h}[\Phi_0(B) - \Phi_i(B)]\frac{h}{2} \end{aligned}\right| \; i = 2, 4$$

$$\left.\begin{aligned} j_{iA} &= \frac{\kappa_A}{h}[\Phi_0(A) - \Phi_i(A)]h \\ j_{iB} &= \frac{\kappa_B}{h}[\Phi_0(B) - \Phi_i(B)]h \end{aligned}\right| \; i = 1, 3 \qquad (6)$$

setting unity for the hypothetical third (depth) dimension z. The hypothetical currents j_{1A} and j_{3B}, which constitute the current going across the interphase, can be eliminated by means of the summation

$$\sum_{i=1}^{4} j_{iA} = \sum_{i=1}^{4} j_{iB} = 0 \qquad (7)$$

This yields

$$\sum_{i,i\neq 1} j_{iA} = -j_{1A}; \quad \sum_{i,i\neq 3} j_{iB} = -j_{3B} \qquad (8)$$

Then we have, for the interphase electrolyte/electrode

$$j_{1A} = -j_{3B} = j \qquad (9)$$

while for the interphase electrode/insulator and

electrolyte/insulator, respectively, the currents

$$\sum_{i,i\neq 1} j_{iA} = 0; \quad \sum_{i,i\neq 3} j_{iB} = 0 \tag{10}$$

respectively, go to zero.

For field continuity we set $A_0 = B_0$. Substituting Equation 6 in Equations 9 or 10, respectively, the interfacial current j is expressed as a function of the potentials $\Phi_i(A)$ and $\Phi_i(B)$. The above holds for a straight edge, but can be developed analogously for the inner and outer corners; for these, the form of Equation 6 changes and the mesh star (compare Figs 4c and 4d) loses some points.

For the interphase electrolyte/insulator the approximations of Equation 4 have the following forms: an edge (Fig. 4b) as

$$4\Phi_0 = 2\Phi_1 + \Phi_2 + \Phi_4 \tag{11}$$

an inner corner (Fig. 4c) as

$$4\Phi_0 = 2\Phi_1 + 2\Phi_4 \tag{12}$$

and an outer corner (Fig. 4d) as

$$6\Phi_0 = 2\Phi_1 + \Phi_2 + \Phi_3 + 2\Phi_4 \tag{13}$$

In all cases, Equations 6 were substituted into Equation 10. For electrode corners or electrode edges, Equation 6 should be substituted into Equation 9.

There are alternative ways of deriving these discretizations, some of which produce slightly different results at corners; since such points are relatively few in number, this will not matter.

Computation proceeds as a sequence of iterations. At each iteration, all mesh points are updated, using Equation 5

$$\Phi_0' = (\Phi_1 + \Phi_2 + \Phi_3 + \Phi_4)/4 \tag{14}$$

where Φ_0' is the new point, often written as $\Phi_0(n+1)$, indicating the next iteration step. Note that our symbol is not to be confused with a derivative. Upon a sufficient number of iterations, the boundary conditions force the field towards a steady state, where the potentials no longer change, that is, the discrete forms of the Laplace equation, Equations 5 and 1 to 13, are satisfied everywhere where appropriate.

The straight use of the above discrete approximations leads to rather extended computation times. It is standard practice to employ overrelaxation: for example, the change $\Phi_0' - \Phi_0$ at a given point at one iteration with Equation 14 is increased by a factor α, changing that equation to

$$\Phi_0' = \frac{\alpha}{4}(\Phi_1 + \Phi_2 + \Phi_3 + \Phi_4) - (\alpha - 1)\Phi_0 \tag{15}$$

with $1 \leqslant \alpha < 2$.

In simple systems, overrelaxation [4, 5] greatly speeds convergence and was used in the homogeneous phases in the present work. The determination of the optimum α value has been described [5].

The special problems arising in the present context are the boundary conditions at the electrolytic double layer interphases. Discretization here must take the following conditions into account: (i) field continuity between the two phases; (ii) the Butler–Volmer (i, Φ) relation.

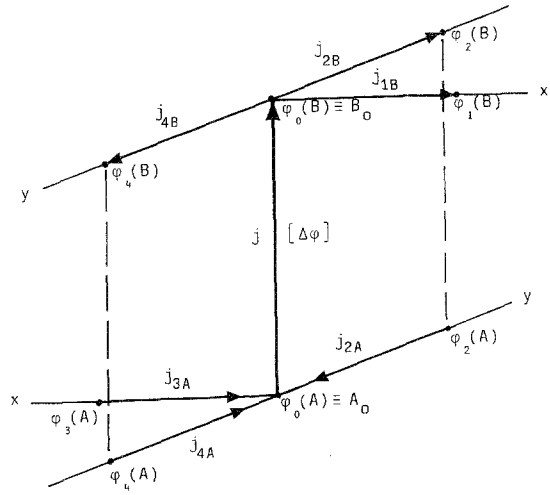

Fig. 5. Schematic of the kinetic current j between the potential points A_0 (Φ_0, phase A) and B_0 (Φ_0, phase B).

Figure 5 shows the situation at the plate/electrolyte (A/B) interface. The interface runs along the y-axis, the x-axis is normal to this interface and the vertical axis represents the potential. There is a potential jump $\Delta\Phi$ across the double layer (assumed to have zero thickness) and, besides currents normal to the interface (j_{3A} and j_{1B}), we must allow for currents flowing tangential to the interface in both phases A and B. By Kirchhoff's rule, the sum of tangential and normal currents at a point A_0 in phase A must equal the corresponding sum in phase B at the point B_0, separated from A_0 by the double layer thickness. Thus, we get the continuity Equation 9 in the form of

$$j_{2A} + j_{3A} + j_{4A} = j_{1B} + j_{2B} + j_{4B} = j \tag{16}$$

Let the ratio K of the conductivities of the two phases A and B be

$$K = \frac{\kappa_A}{\kappa_B} \tag{17}$$

with κ the conductivities of the phases. Writing A_i for $\Phi_i(A)$ and B_i for $\Phi_i(B)$, Equation 16 leads to the continuity condition

$$2B_1 + (B_2 + KA_2) + 2KA_3 + (B_4 + KA_4) = 4(B_0 + KA_0) \tag{18}$$

when we substitute Equations 6 into it.
Using the identities

$$2B_1 \equiv \Omega_1; \quad B_2 + KA_2 \equiv \Omega_2; \quad 2KA_3 \equiv \Omega_3; \quad B_4 + KA_4 \equiv \Omega_4; \quad B_0 + KA_0 \equiv \Omega_0 \tag{19}$$

Equation 18 becomes

$$\Omega_1 + \Omega_2 + \Omega_3 + \Omega_4 = 4\Omega_0 \tag{20}$$

which is identical in form with Equation 5, so we have the equivalent of Equation 14

$$\Omega_0' = (\Omega_1 + \Omega_2 + \Omega_3 + \Omega_4)/4 \tag{21}$$

as well as (in principle) the overrelaxation form, Equation 15

$$\Omega_0' = \frac{\alpha}{4}(\Omega_1 + \Omega_2 + \Omega_3 + \Omega_4) - (\alpha - 1)\Omega_0 \quad (22)$$

The expression Ω_0' calculated from Equation 22, however, has a meaning different from the new potential, Φ_0', in Equation 15. It is an algebraic operator which introduces the information in the Butler–Volmer relation and had the following forms, in the case of the hydrogen and oxygen electrodes

$$H_2: \Omega_0' = B_0(1 + K) - \frac{2RTK}{F}\sinh^{-1}\left(\frac{\kappa_B(2B_1 + B_2 + B_4 - 4B_0)}{4hi_{OH_2}}\right) \quad (23)$$

$$O_2: \Omega_0' = B_0(1 + K) + KU_0 + \frac{2RTK}{F}\sinh^{-1}\left(\frac{\kappa_B(4B_0 - B_2 - 2B_3 - B_4)}{4hi_{0O_2}}\right) \quad (24)$$

The derivation of Equation 23 and 24 proceeds as follows. For the hydrogen and oxygen electrodes, respectively, Equation 3 can be written as (cf. Fig. 2)

$$\Delta\Phi_c = -\eta_c = \Phi_{s,c} - \Phi_{m,c} = \frac{2RT}{F}\sinh^{-1}\left(\frac{i}{2i_{OH_2}}\right) \quad (25)$$

$$\Delta\Phi_a = \eta_a + U_0 = \Phi_{m,a} - \Phi_{s,a} = U_0 + \frac{2RT}{F}\sinh^{-1}\left(\frac{i}{2i_{0O_2}}\right) \quad (26)$$

using the Butler–Volmer relations. In these equations, transport effects were neglected, which is not unreasonable in the case of an electrolyser as assumed here.

Identifying the potentials Φ_m in the metal phase with $\Phi_0(A) \equiv A_0$ and Φ_s in the solution phase with $\Phi_0(B) \equiv B_0$, we obtain from Equations 25 and 26 the equations

$$B_0 = A_0 + \frac{2RT}{F}\sinh^{-1}\left(\frac{i}{2i_{OH_2}}\right) \quad (25a)$$

$$A_0 = B_0 + U_0 + \frac{2RT}{F}\sinh^{-1}\left(\frac{i}{2i_{0O_2}}\right) \quad (26a)$$

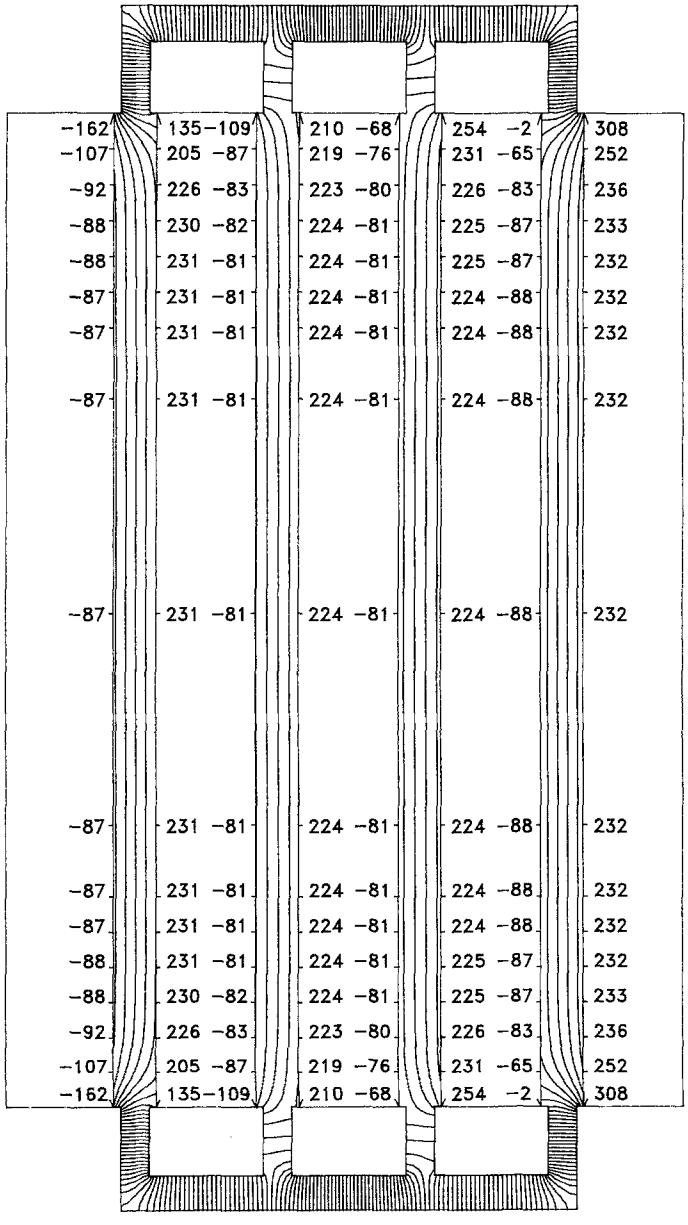

Fig. 6. Potential profile of a bipolar water electrolyser. Current density at the end plates: 4000 A m^{-2}. The negative numbers show the cathodic overpotentials η_{H_2}(mV); the positive numbers show the anodic overpotentials η_{O_2}(mV).

The local current density i in these equations has dimension $A\,m^{-2}$. It can therefore be calculated from the local currents j_{1A} and j_{3B} in Equations 6 and 9 (the dimension of j is A), by dividing the respective expression for j in Equation 9 by the element area hl (or $\frac{1}{2}hl$), according to the geometry of the finite-difference element (edge or corner). In this way the expressions

$$i = \frac{j}{h/2}, \quad i = \frac{j}{h} \tag{27}$$

respectively, are obtained for the current density i. Just as in the derivation of Equation 8, the depth coordinate z was set at unity hl or $\frac{1}{2}hl$. By substituting 9 and 27 into 25a and 26a and noting that

$$B_0 + KA_0 = \Omega_0 \tag{28}$$

Equations 23 and 24 are obtained. (i_{OH_2} and i_{0O_2} are the respective exchange current densities and h the previously defined interval in both x and y). Combining Equation 22 with Equations 23 and 24, the calculated value Ω_0' then yields the overpotentials η_a for the oxygen and η_c for the hydrogen reaction in the form of Equation 2 and 3, using the known Butler–Volmer relation, assuming negligible transport effects

$$H_2: i = 2i_{OH_2} \sinh\left(\frac{F(B_0 - A_0)}{2RT}\right) \tag{29a}$$

$$O_2: i = 2i_{0O_2} \sinh\left(\frac{F(A_0 - B_0 - U_0)}{2RT}\right) \tag{29b}$$

Equations 29a and 29b correspond to Equations 25a and 26a, respectively. Previous efforts [7] have avoided the nonlinearity of the Butler–Volmer relation by approximating it by a linearization around working potentials. Rousar *et al.* [9], in fact, state that the nonliner relation leads to instabilities in the calculation; this was found not to be true in the present work, and the use of the correct Butler–Volmer form was preferred.

The calculation of the local thermodynamic stabilities of individual cell elements should be feasible even for stacks of up to 50 units. For this reason, a rapidly converging computation method is required. This is obtained by the use of overrelaxation (Equation 15), although it was found that at the interfaces, α needed to be set equal to unity in Equation 22, which amounts to the use of Equation 21, or no overrelaxation. It is clear from Equation 22 that overrelaxation allows only the operators Ω_i to converge, as a whole. As seen from the definitions, however, (Equation 19), the

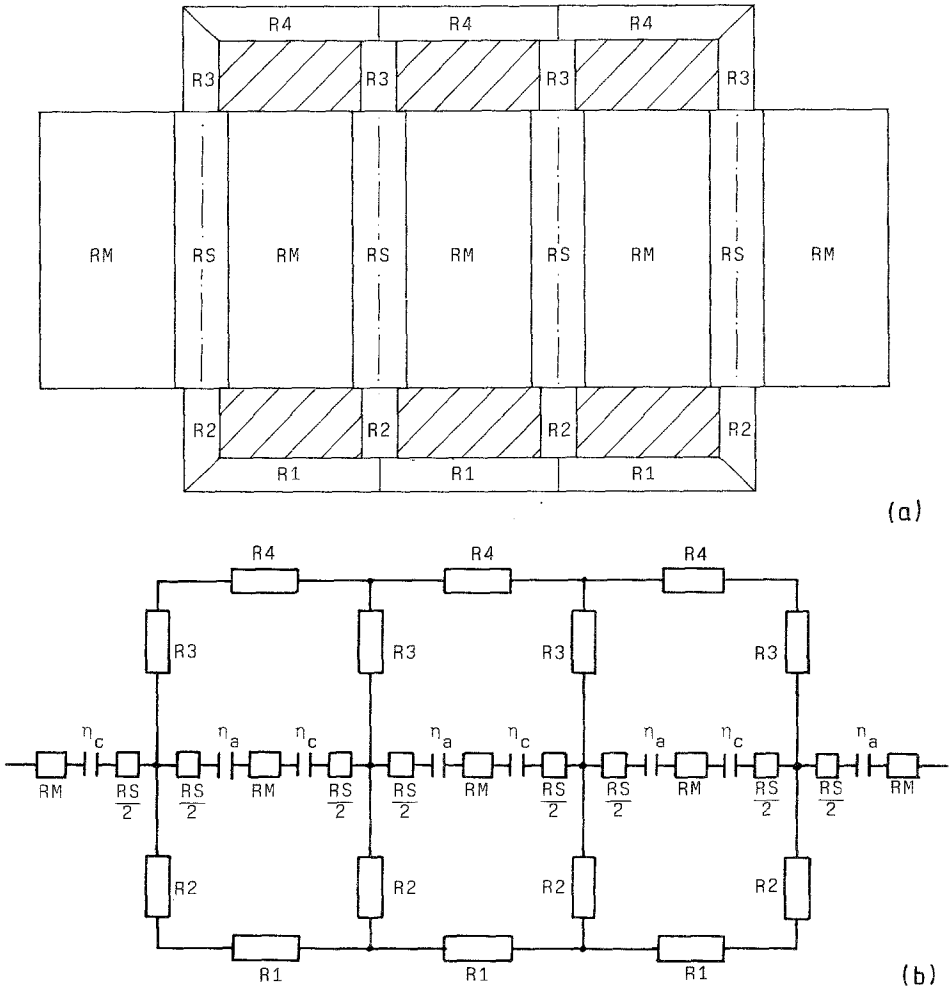

Fig. 7. Two-dimensional schematic of the bipolar electrolyser (a) and its transformation to a circuit analog model (b).

Table 1. Input data for the model electrolyser

	R (Ω)	d (m)	l (m)
R1	2.375	0.005	0.019
R2	1.563	0.004	0.010
RS	0.022	0.170	0.006
RM	4.8×10^{-6}	0.170	0.014
R3	1.563	0.004	0.010
R4	2.375	0.005	0.019

Metal resistivity, ϱ : 0.005 Ω m
Electrolyte resistivity, ϱ : 62.5 Ω m
Temperature : 373 K
Current density : 4000 A m^{-2}
i_0 hydrogen : 1000 A m^{-2}
i_0 oxygen : 100 A m^{-2}
Overrelaxation factor α : 1.75
Error limit for an iteration : 10^{-8} relative
U_0 : 1.167 V

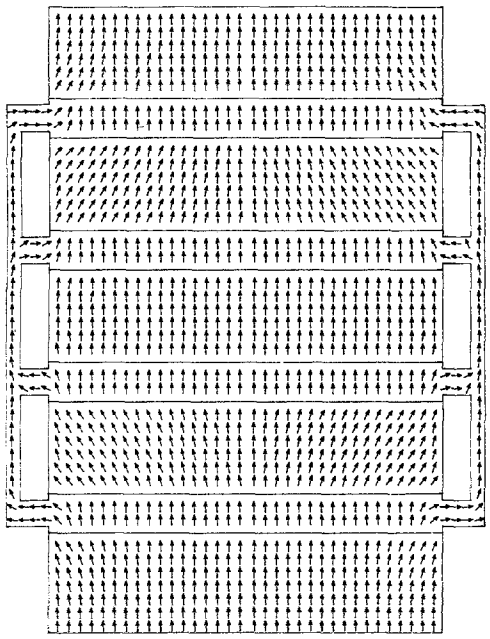

Fig. 8. Vectorial representation of current flow in a bipolar water electrolyser with three bipolar plates. Working mode corresponds to Fig. 6.

actual B_i terms will converge with Ω_i, while the A_i are all multiplied by the conductivity ratio K; that is, the A_i terms converge more slowly by a factor K. For large values of K, which is the case with metallic plates, convergence is then unacceptably slow and would limit the simulations to cell blocks with only a few plates. Two strategies were tried out to overcome this problem:

(i) The potential field in the electrodes was assumed to be homogeneous although variable; thus the same potential holds everywhere within a plate. One can thus, initially, consider the plate as two adjacent double layers and take the total current at a point on one side to be equal to the total current emerging from the other at the same plate height (y), adding the Butler–Volmer potential jumps appropriately. The plate itself is thus left out entirely at this stage. Upon convergence, this restriction was relaxed and more iterations computed using the proper boundary conditions, (Equations 16 to 24), yielding the curved potential fields within the plates as well. Since this is the sequential coupling of two only moderately converging processes, this strategy is suitable for cells with only up to about 10 bipolar plates.

(ii) The electrolyser was modelled as a network of voltage sources and resistances, all linear in the homogeneous phases, as in [6], while the Butler–Volmer relation was allowed at the interfaces. The current density at the end plates was set to a certain value (e.g. 4000 A m^{-2}). This scheme can be rapidly calculated by the mesh current method, using the Levenberg–Marquardt algorithm [10, 11] for resistive networks. A good approximation of both potential distribution and the total cell voltage is obtained which, by interpolation into a finer mesh, can then be used as the starting state for the actual FDM iterations for the Laplace equation. With this method, the

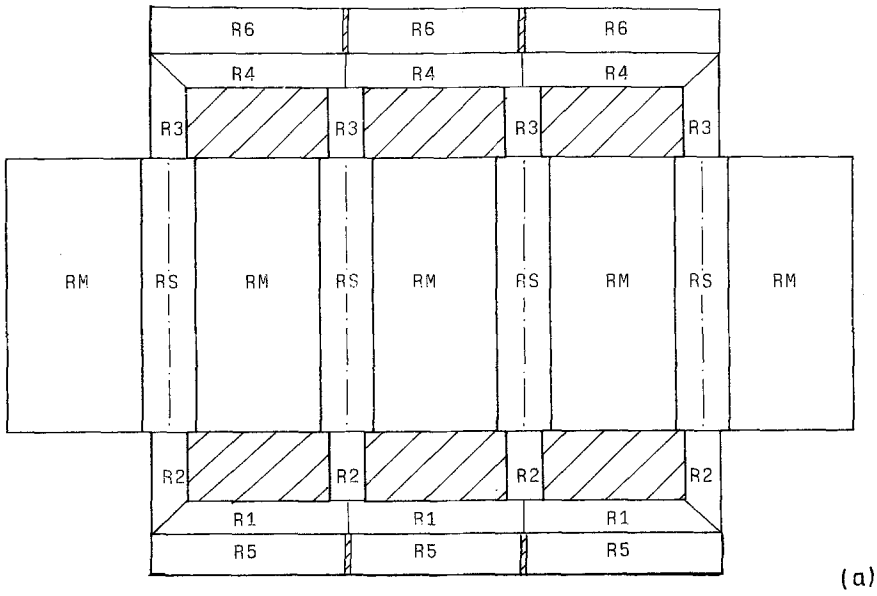

Fig. 9. Two-dimensional schematic of a bipolar electrolyser with conducting manifolds (a) and its transformation into a circuit analog model (b). The unit sections of the conducting manifold are electrically insulated from each other so that they function as bipolar elements.

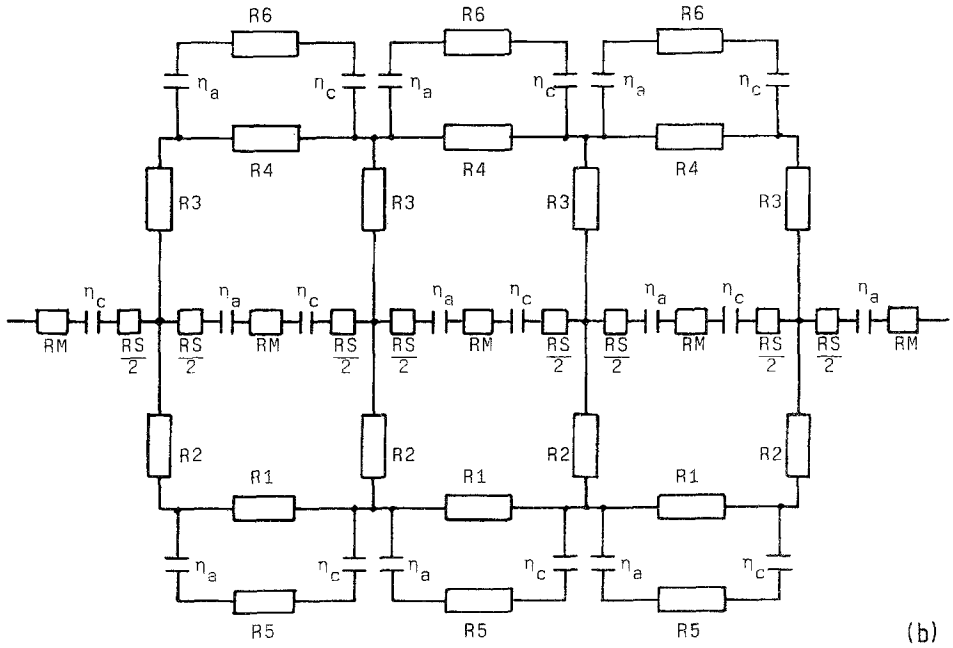

Fig. 9. Continued

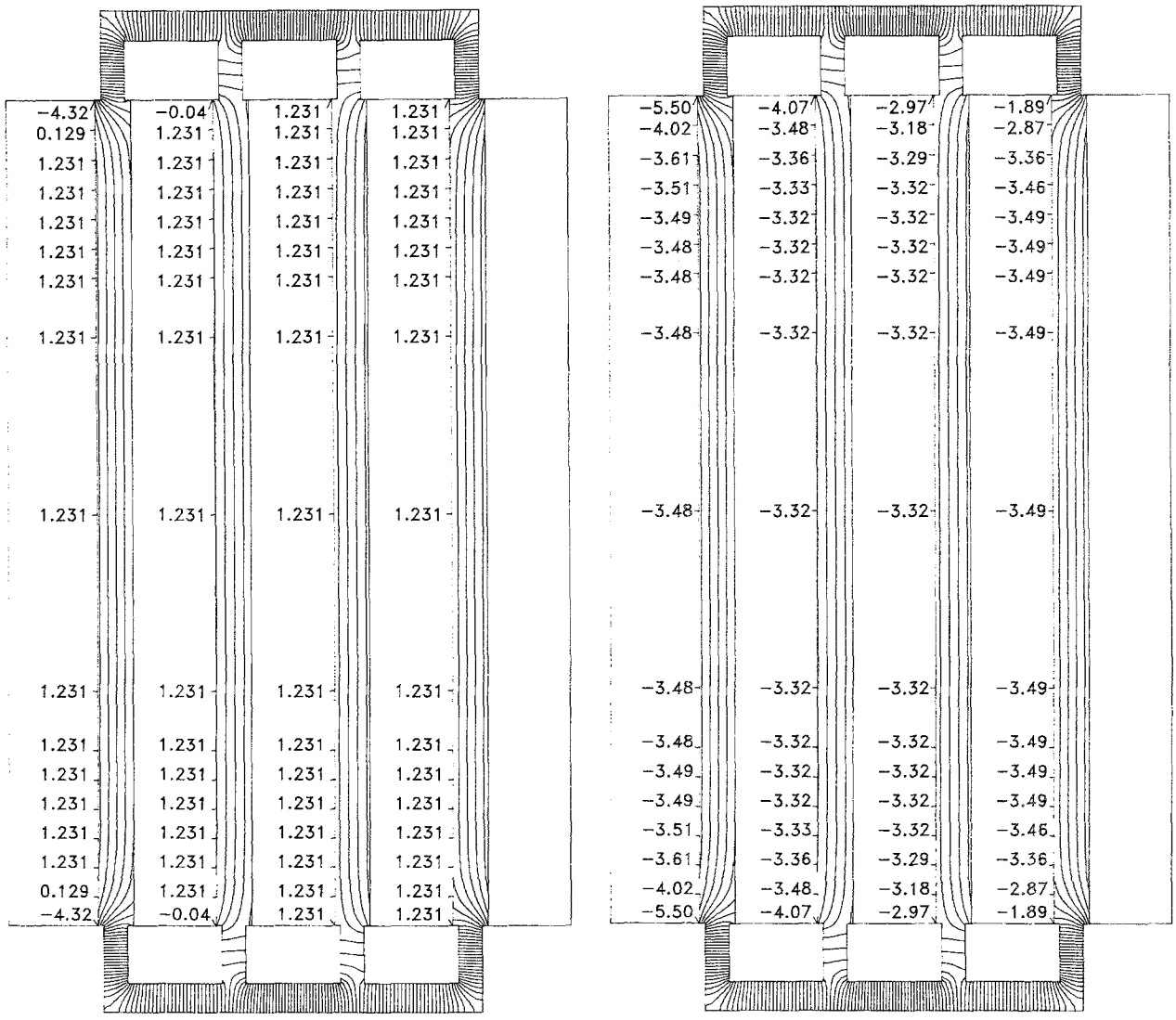

Fig. 10. Topological picture of corrosion sites in the bipolar electrolyser at 100° C in 12 m (10 M) KOH. Current density at the end plates was 4000 A m^{-2}. Input parameters are listed in Table 1. The numbers indicate the metal solubility as log m (molality). (a) Mo (pure phase); (b) Fe (pure phase).

number of iterations required is so small that large bipolar systems with 50 units can be simulated with reasonably short computing times. Nguyen and White [12] have used a different method of speeding up computations: In principle, the discrete expressions shown above, Equations 5 and 11 to 14 and the interface discretizations, applied to all mesh points, result in a huge matrix equation. The matrix is, however, strongly banded, being mostly pentadiagonal. These authors utilized this property and some mathematical devices to solve the matrix equation with a standard band matrix solver. It is not clear, however, whether this is applicable in the present context, in view of the rather complex geometry of a bipolar cell stack.

By means of the above discrete equations, the entire cell mesh can be solved. Convergence was defined as that point, at which the maximum absolute change for all points was below some present limit, usually 10^{-8} relative to the total applied cell voltage. Programming is straightforward; the computations were carried out using an IBM 370 computer in double precision, coding in FORTRAN.

4. Results and discussion

The two strategies (i) and (ii) yield almost identical results. Calculations were checked against measured potentials in a bipolar cell block [11] and good agreement was found.

Figure 6 shows the potential profile in a cell block with three bipolar plates. The geometrical data, resistances and their transformation into a circuit analog model (Fig. 7) are seen in Table 1. The vectorial representation of current flow is shown in Fig. 8.

The method is also usable for bipolar electrolysers with conducting manifolds. In this case, the circuit analog model is extended by the currents flowing through the manifold walls, as shown, for example, by Burney and White [13]. Figure 9 shows the corresponding cell schematic and its transformation into an analog model. The computational difficulties are considerable in this case, however. For this reason, the direct use of multigrid techniques has to be preferred, as will be shown in the next contribution.

When the potential distribution along the electrode edges, in the form of overpotentials, is known (see

Table 2. Potential values and local stabilities of Fe and Mo in a bipolar stack with 60 units

Plate no.	*Main current density* ($A\,m^{-2}$)	*Local current density* ($A\,m^{-2}$)			*Local overvoltage* (V)		
		Lower corner	*Central part*	*Upper corner*	*Lower corner*	*Central part*	*Upper corner*
0 cath.	−4030	−13170	−3710	−13170	−0.166	−0.089	−0.166
1 anod.	3530	730	3710	730	0.129	0.232	0.129
cath.	−3470	−6400	−3370	−6400	−0.121	−0.083	−0.121
2 anod.	3300	2200	3370	2200	0.199	0.226	0.199
cath.	−3300	−4560	−3260	−4560	−0.100	−0.081	−0.100
5 anod.	3220	3610	3220	3610	0.231	0.223	0.231
cath.	−3220	−3750	−3210	−3750	−0.089	−0.080	−0.089
30 anod.	3220	3680	3210	3680	0.232	0.223	0.232
cath.	−3220	−3720	−3210	−3720	−0.089	−0.080	−0.089
55 anod.	3220	3720	3210	3720	0.232	0.223	0.232
cath.	−3220	−3640	−3220	−3640	−0.087	−0.081	−0.087
58 anod.	3300	4470	3260	4470	0.244	0.224	0.244
cath.	−3300	−2050	−3370	−2050	−0.058	−0.083	−0.058
59 anod.	3470	6220	3730	6220	0.266	0.226	0.266
cath.	−3520	100	−3730	100	0.003	−0.089	0.003
60 anod.	4030	12750	3730	12750	0.312	0.233	0.312

Cathode no.	*log m Fe*			*log m Mo*		
	Lower corner	*Central part*	*Upper corner*	*Lower corner*	*Central part*	*Upper corner*
0	−5.601	−3.520	−5.601	−4.606	1.231	−4.606
1	−4.385	−3.358	−4.385	−0.958	1.231	−0.958
2	−3.818	−3.304	−3.818	0.744	1.231	0.744
5	−3.520	−3.277	−3.520	1.231	1.231	1.231
30	−3.520	−3.277	−3.520	1.231	1.231	1.231
55	−3.466	−3.304	−3.466	1.231	1.231	1.231
58	−2.683	−3.358	−2.683	1.231	1.231	1.231
59	−1.894	−3.520	−1.894	1.231	1.231	1.231

Fig. 6), then the thermodynamic solubilities of the relevant metals (Fig. 1) can be topologically introduced into the electrolyser as a function of this potential distribution. The characteristic properties of these stabilities are expressed in terms of the potential dependence of the solubilities under the working conditions (temperature, pressure, electrolyte concentration). This was calculated, making use of the Criss–Cobble correspondence principle [14, 15]; for example, for Mo (catalyst) and Fe (construction material) the formulas are

$$\log m_{HFeO_2^-} = -1.115 + 27.023\,\eta_{H_2} \quad (30)$$

$$\log m_{MoO_4^{2-}} = 8.851 + 81.069\,\eta_{H_2} \quad (31)$$

Equations 30 and 31 are valid for pure phases at 5 atm (pressure electrolysis) and 100° C in 10 M KOH. If Equation 3 is substituted in Equations 30 and 31, then a direct topological picture of local stability of the various materials in the bipolar stack can be obtained, as well as the potential profile (see for example Fig. 10, showing a system of 4 units). A corresponding assignment to a stack with 60 units is contained in Table 2.

5. Conclusions

By the numerical solution of the Laplace equation for the potential field in the region of a bipolar electrolysis block, potential profiles can be obtained which, in conjunction with the Pourbaix diagrams for the relevant metals (catalysts, construction materials), enable the determination of those zones in an electrolyser endangered by corrosion. We have been able to show that a combination of a circuit analog model of the electrolyser and the discretized Laplace equation makes it possible to compute the potential field even for large bipolar cell blocks in two-dimensional space. The method can be used in a sufficiently wide current density range, so that both fully loaded and depolarized conditions of the system can be calculated. Thus, for example, intermittently operating electrolysers powered by solar energy can be better designed.

Acknowledgement

We thank Dr B. Steffen for fruitful discussions concerning the convergence problems.

References

[1] M. Jaksic, *Electrochim. Acta* **29** (1984) 1539.
[2] J. Divisek and J. Balej, to be published in DECHEMA-Monographien 1990.
[3] J. Divisek and H. Schmitz, 'Galvanische Herstellung und elektrochemische Stabilität von aktiven Nickelelektroden', DECHEMA-Monographie, 1989, p. 299.
[4] L. Lapidus and G. F. Pinder, 'Numerical Solution of Partial Differential Equations in Science and Engineering', Wiley, New York (1982) pp. 34–48.
[5] D. Britz, 'Digital Simulation in Electrochemistry', 1st edn, Springer, Berlin (1980).
[6] C. J. H. King and D. E. Danley, 'Experimental Measurement of Current Leakage in a Commercial Scale Bipolar Cell Stack', The Electrochemical Society Extended Abstracts, May 1982. (Cited in [7].)
[7] J. W. Holmes and R. E. White, in 'Electrochemical Cell Design' (Ed. R. E. White), Plenum, New York (1984) p. 311.
[8] E. C. Dimpault-Darcy and R. E. White, *J. Electrochem. Soc.* **135** (1988) 656.
[9] I. Rousar, K. Micka and A. Kimla, 'Electrochemical Engineering', Elsevier, Amsterdam (1986).
[10] J. Divisek, J. Mergel and H. Schmitz, 'Advanced water electrolysis cell in discontinuous operation mode', in Hydrogen Energy Progress VII edited by T. N. Veziroglu and A. N. Protsenko, Pergamon, Oxford (1988) p. 327.
[11] J. Divisek and L. Fürst, 'Ermittlung des Potentialprofils in einem bipolaren Elektrolyseur', DECHEMA-Monographie 1989, p. 245.
[12] T. V. Nguyen and R. E. White, *Comput. Chem. Engng.* **11** (1987) 543.
[13] H. S. Burney and R. E. White, *J. Electrochem. Soc.* **135** (1988) 1609.
[14] C. M. Criss and J. W. Cobble, *J. Am. Chem. Soc.* **86** (1964) 5385.
[15] *Idem, ibid.* **86** (1964) 5390.